MECHANICAL BEHAVIOUR AND FAILURE CRITERION OF TI-6AL-4V ALLOY AT ROOM AND CRYOGENIC TEMPERATURES

G. LAURENT, G. CAILLETAUD, L. REMY.
Ecole Nationale Supérieure des Mines de Paris - Centre des Matériaux
URA CNRS 866 B.P. 87 - 91003 EVRY Cedex - FRANCE

ABSTRACT

The effects of the stress triaxiality on mechanical behaviour and failure criterion at room and cryogenic temperature were investigated for ELI grade Ti-6Al-4V alloy using notched bars. Tensile tests and cyclic stress-strain tests were performed on cylindrical specimens at 300 K and 50 K. Tests results allowed the determination of the material viscoplastic behaviour law by the means of an inverse method.The purpose of this paper is twofold : firstly to study the influence of the stress concentration and stress triaxiality on tensile fracture strength at room temperature and at 50 K in liquid helium environment using cylindrical notched specimens; secondly to investigate a failure criterion of TA6V (ELI) using the analysis of fracture surfaces and computer simulation.

KEYWORDS

ELI grade Ti-6Al-4V alloy, room and cryogenic temperatures, viscoplasticity, ductile failure criterion, tensile test, constitutive equation, finite element method.

1 INTRODUCTION

Launch vehicles Ariane 5 are powered by cryogenic engines that use liquid O_2 and H_2. In these motors and especially in the turbo-pumps, some parts run at low temperature : 20 K when in contact with H_2, 90 K with O_2. The impellers of H_2-turbo-pump are made of Ti-6Al-4V. The extra low interstitial Ti-6Al-4V alloy is used for cryogenic application, since the reduction of interstitial concentration causes an increase in toughness of titanium alloys.
After a brief presentation of this material and experimental procedure, the results of tensile tests and cyclic stress-strain tests at room and cryogenic temperature and the analysis of fracture surfaces are presented in the next section. The results of monotonic and cyclic stress-strain tests on smooth specimens form a data base allowing the identification of constitutive equations by means of an inverse method. The third section presents the computation of the stress and strain field in notched specimens by a F.E. code using the previous viscoplastic model, at 300 K and 50 K. The fourth section presents a numerical simulation of fracture. The model proposed by Rice and Tracey for cavity growth was then applied to fracture prediction, since fractographic examination reveals the presence of numerous cavities on grain boundaries,.

2 EXPERIMENTAL PROCEDURE

The material used for this study is a titanium base alloy, ELI grade Ti-6Al-4V, which can be used for cryogenic components of turbo-pumps. Test-specimens (described in next section) were cut by electro-discharge machining from a 130 mm diameter cast bar. This alloy exhibits a typical two-phase (α+β) structure titanium alloy: a compact hexagonal structure (alpha phase) and a body centered cubic (beta phase). The chemical composition of TA6V ELI is listed in table 1.

Material	Chemical composition						
TA6V ELI	Al	V	Fe	O	C	N	Ti
(weight %)	6.16	4.16	0.19	0.11	0.02	0.009	Bal.

Table 1 : Chemical composition of TA6V ELI.

The microstructure of this alloy is an equiaxed globular structure. Three distinct phases can be observed : the grain size of α phase (hcp) is approximately 10-25 µm, the α' phase being in the form of plates (1 µm in thickness and 5-15 µm in length). These plates are arranged in small clusters of 4 to 10 plates having the same crystallographic orientation. The α' phase is embedded in a body centered cubic matrix (β phase). Figure 1 shows optical micrographs of TA6V ELI in the sampling region of specimens.

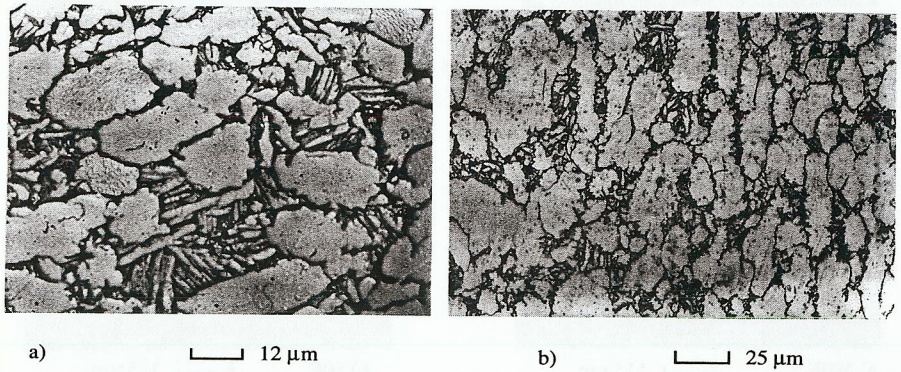

a) 12 µm b) 25 µm

Fig. 1: Optical micrographs of TA6V ELI. Photographs are perpendicular to the axis of the cast bar (a) and (b) parallel to the axis of the cast bar respectively.

The test-specimens geometries are shown in figure 2. The notched specimens geometries were chosen so that the stress concentration factor (K_t) varies from 1.6 to 3.23. These values of K_t were reached with a U notch (K_t = 1.6 and 2.00) or a V notch (K_t = 3.23). The smooth specimens for tensile test and stress-strain test were mechanically polished parallel to their longitudinal axis using diamond paste down to 3 µm and were then observed by optical microscopy in order to detect surface cracks and defects before testing.

Tensile tests and hardening tests at 50 K were conducted in regulated liquid helium cryostat as shown in figure 3. Temperature was controlled by a thermocouple welded on the specimen head. Tensile tests were performed at 300K and 50K at a strain rate of about $\dot{\varepsilon}_t = 10^{-4} s^{-1}$. The

strain, stress, time and displacement were recorded using a micro-computer. For each temperature, two or three tests were carried out and a variation of 1.5-2.5% was found. Cyclic stress-strain tests were performed at a frequency of 0.1 Hz and the strain ratio ($R_\varepsilon=\varepsilon_{min}/\varepsilon_{max}$) was R_ε=-1. The strain was increased by increments after stress-stabilisation was achieved. For each strain level, ten cycles are required to obtain the hardening curves.

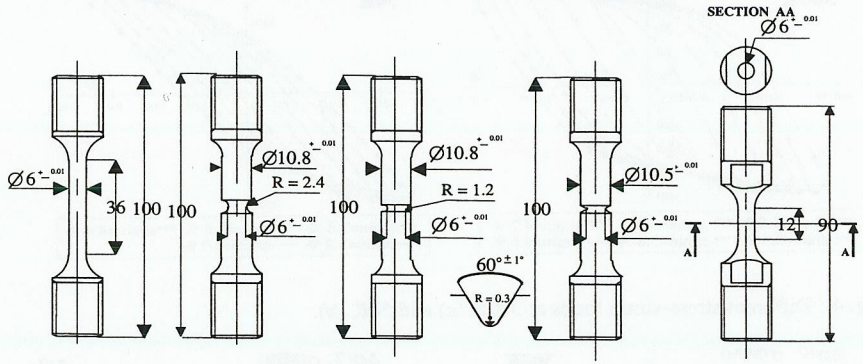

Fig. 2 : Specimen geometries (in mm).

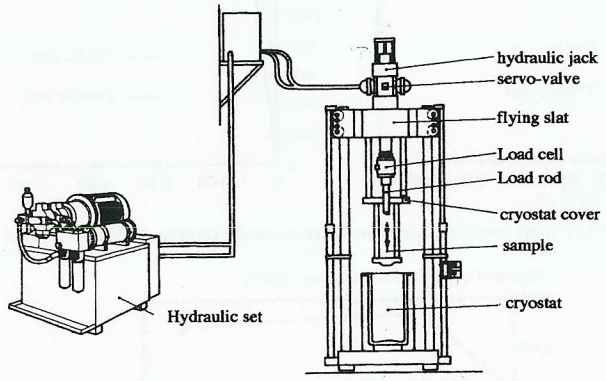

Fig. 3 : Material testing facility at 50K in liquid helium.

3 EXPERIMENTAL RESULTS

The results of stress-strain tests disclosed cyclic softening in TA6V ELI. Different cyclic stress-strain loops are shown in figure 4 and a comparison between the tensile curves and cyclic stress-strain curves at 300K and 50K is shown in figure 5.

The tensile tests were performed in order to investigate the effect of stress concentration. The evolution of nominal ultimate tensile stress to fracture versus K_t shows two different curves at each temperature in figure 6. At 300K, this stress increases with K_t but at 50K, it increases until $K_t = 2.00$ and then decreases for higher values of K_t.

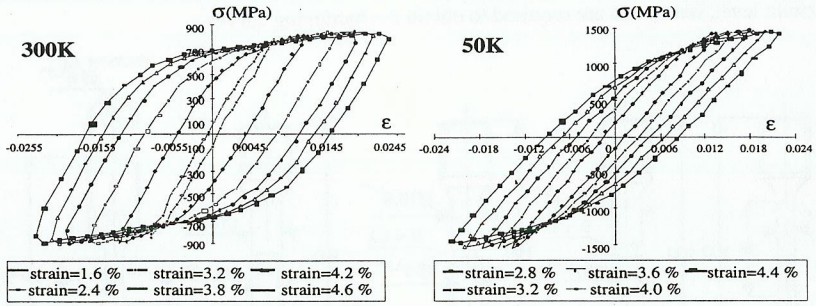

Fig. 4 : Different stress-strain loops at 300K (a) and 50K (b).

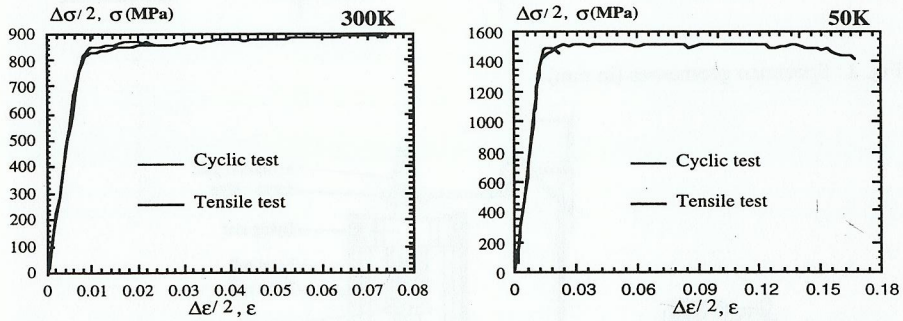

Fig.5 : Comparison between tensile curves and stress-strain curves at 300K (a) and 50K (b).

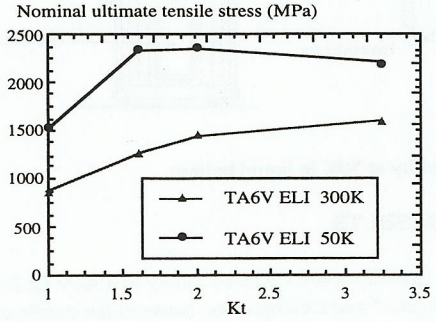

Fig. 6 : Evolution of nominal stress versus K_t at 300K and 50K.

Metallographic observations were carried out on all specimens tested. Figure 7 illustrates the fracture surfaces of TA6V ELI tested at room and low temperatures, using a scanning electron microscope (SEM). Micrographs (Fig. 7a) display an intergranular fracture mode with numerous cavities on grain boundaries, indicating a typical grain boundary ductile fracture. Meanwhile at low temperature, the fracture surface (Fig. 7b) exhibits mixed fracture modes : intergranular ductile fracture and transgranular fracture.

Moreover, SEM observations of metallographic section under the fracture surface were made which have shown the presence of cavities with a diameter of 1 to 15 µm. These cavities are located in the interface between alpha and beta phases (figures 8a and 8b). No cavity can be observed any more, beyond 0.5 mm from the fracture surfaces.

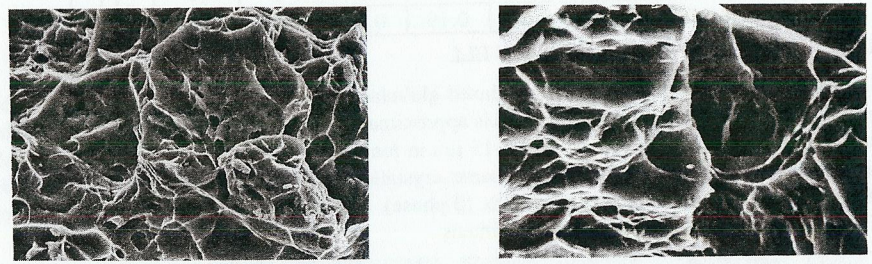

a) 300K ⌊—⌋ 20 µm b) 50K ⌊—⌋ 17 µm

Fig. 7 : Fracture surface of tensile test-specimens at 300K (a) and 50K (b).

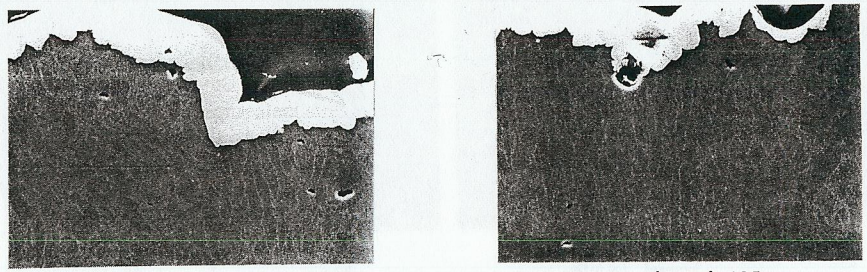

a) 300K ⌊—⌋ 115 µm b) 50K ⌊—⌋ 125 µm

Fig. 8 : Metallographic section under the fracture surface at 300K (a) and 50K (b).

4 MECHANICAL ANALYSIS

The material parameters of the viscoplastic constitutive equations at 300K and 50K are found by means of the code SiDoLo (Pilvin, 1988), using tensile and cyclic stress-strain tests results. A viscoplastic Chaboche model with internal variables was used to simulate the stress-strain behaviour of this titanium alloy [Chaboche, 1977; Lemaitre and Chaboche, 1988). The strain is partitioned into an elastic and a viscoplastic part: $\underset{\sim}{\varepsilon} = \underset{\sim}{\varepsilon}^e + \underset{\sim}{\varepsilon}^v$ (1)

The elastic domain is defined by means of a von Mises equivalent, introducing both kinematic X and isotropic R hardening, so that:

$$f\left(\underset{\sim}{\sigma},\ \underset{\sim}{X},\ R\right) = J\left(\underset{\sim}{\sigma} - \underset{\sim}{X} - 1.5\ C_1\ \underset{\sim}{\varepsilon}^v\right) - R - \sigma_y \qquad (2a)$$

with $J(\underset{\sim}{\sigma}-\underset{\sim}{X})=\sqrt{1.5(\underset{\sim}{\sigma}-\underset{\sim}{X})^{dev}.(\underset{\sim}{\sigma}-\underset{\sim}{X})^{dev}}$ (2b)

The viscoplastic flow is governed by the normality rule, so that: $\dot{\underset{\sim}{\varepsilon}}^{v}=\dot{v}\,\underset{\sim}{n}$ (3)

with $\dot{v}=\left\langle\frac{f}{K}\right\rangle^{n}$, (using $\langle H\rangle=\max(H,0)$) and $\underset{\sim}{n}=\frac{\partial f}{\partial\underset{\sim}{\sigma}}=\frac{3}{2}(\underset{\sim}{\sigma}-\underset{\sim}{X})^{dev}/J(\underset{\sim}{\sigma}-\underset{\sim}{X})$ (4)

The hardening depends on the state variables $\underset{\sim}{\alpha}$ and v:

$\underset{\sim}{X}=2/3\ C_2\underset{\sim}{\alpha}$ with $\dot{\underset{\sim}{\alpha}}=\dot{\underset{\sim}{\varepsilon}}^{v}-D\underset{\sim}{X}\dot{v}$ and $R=Q(1-e^{-bv})$ (5)

The material parameters are then:

- the initial yield stress σ_y; Q and b defining its variation.
- C and D characterizing kinematic hardening.
- K and n characterizing the viscosity, which is of course very low at these temperatures.
- Young modulus E and the Poisson ratio v.

Typical computations are shown in figure 9 for two stabilized loops at 300K and 50K.

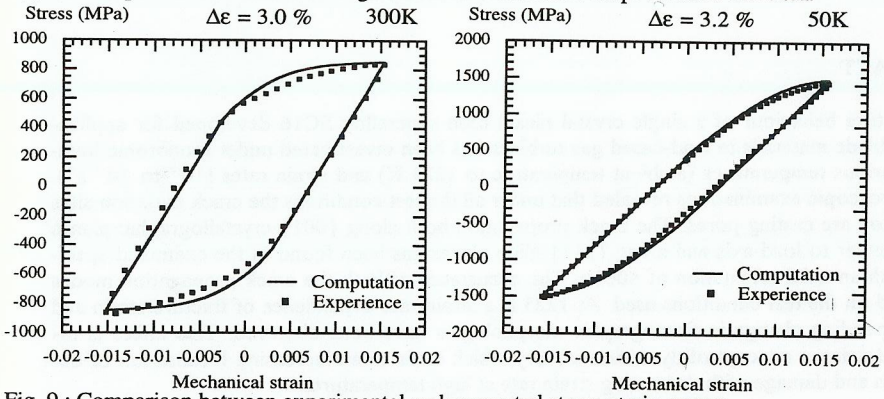

Fig. 9 : Comparison between experimental and computed stress-strain curves.

The identified constitutive equations were used in the finite element (F.E.) code ZeBuLoN to calculate strains and stresses in notched specimens tested to fracture. For symmetry reasons, only one half of the mid section was modelled. The mesh and the boundary conditions for notched-specimens are shown in figure 11. Stress concentration is localized in the notch. When the specimen breaks, the cumulated viscoplastic strain is maximum at notch tip and reached 30.9%, 36.2% and 44.7% for test specimens with K_t = 1.6, 2.00, 3.23 respectively at 300K.

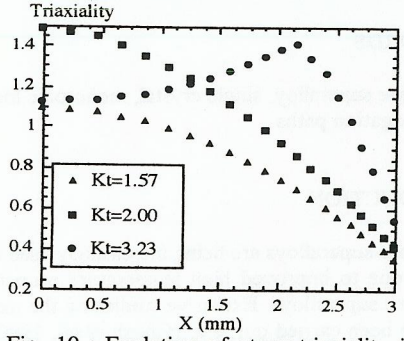

Fig. 10 : Evolution of stress-triaxiality in the minimum section of the specimens when fracture appears at 300K.

Examples of the results for triaxiality obtained at 300K are presented in figure 10 where X (in mm) represents the distance to specimen axis.

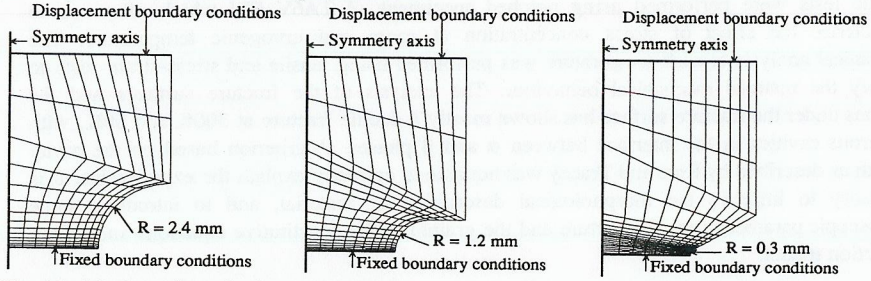

Fig. 11 : Meshes of notched test-specimens.

5 SIMULATION OF FRACTURE

Since the observation of metallographic sections under the fracture surface have shown the presence of numerous cavities, the model of Rice and Tracey (Rice and Tracey, 1969), based on cavity growth and coalescence will be exposed for the TA6V ELI. This model assumes that the fracture occurs in three steps : cavity nucleation, growth of cavities and final fracture by shearing between cavities. According the cavity growth rate is defined through:

$$\frac{dR}{R}=0.283\ .\ \exp\left(\frac{3}{2}\frac{|\sigma_m|}{\sigma_{eq}}\right).\ d\varepsilon^{p}_{eq} \qquad (6)$$

where R is the cavity radius, σ_m is the hydrostatic stress with $\sigma_m=\frac{1}{3}.\mathrm{trace}(\bar{\bar{\sigma}})$

σ_{eq} is von Mises equivalent stress and ε^{p}_{eq} is von Mises equivalent plastic strain.

Ductile fracture is supposed to occur when the ratio of current cavity size R to initial size R_O reaches a critical value $(R/R_O)_C$. This model is applied in a post-processor to treat the previous computations. A critical value $(R/R_O)_C$ is then derived for each specimen type, which is reported in table 2 for 300K. Unfortunately failure does not correspond to a constant value of $(R/R_O)_C$ rate at variance with results on steel (Beremin, 1981; Marini and Mudry, 1985). That demonstrates that this simple criterion is not appropriate for this material. The major reason in the inadequacy of the model is probably the use of assumption of homogeneity of the material, in place of a description of its multi-phase morphology.

Specimens	$\left(\frac{R}{R_0}\right)_c$
U-notch; R = 2.4 mm	1.56
U-notch; R = 1.2 mm	1.49
V-notch; R = 0.3 mm	1.34

Table 2 : Computed critical ratio of cavity growth at 300K (model by Rice and Tracey).

6 CONCLUSION

Tensile tests were performed using notched specimens of TA6V ELI which allow us to characterize the effect of stress concentration at room and cryogenic temperature. The mechanical analysis at each temperature was performed using tensile and stress-strain tests to identify the material mechanical behaviour. The analysis of the fracture surfaces and the sections under the fracture surface has shown mostly a ductile fracture at 300K and 50K, with numerous cavities in the interface between α and β phases. A criterion based on the cavity growth as described by Rice and Tracey was not able to correctly explain the experiments. It is necessary to improve the morphological description of material, and to introduce some microscopic parameters (as the texture and the grains) in the constitutive equations and failure prediction model.

Acknowledgments

Financial support for this study by SEP (Société Européenne de Propulsion) and CNES (Centre National d'Etudes Spatiales) as a part of a research program and cryogenic tests made at SEP are gratefully acknowledged.

References

BEREMIN F.M.; "Study of fracture criteria for ductile rupture of A508 steel", Advances in Fracture Research (ICF5), D. FRANCOIS (ed.), Pergamon press, 1981, p. 809.

CHABOCHE J.-L., Viscoplastic constitutive equations for the description of cyclic and anisotropic behaviour of metals., *Bulletin de l'Académie Polonaise des Sciences*, Série Sc. et Tech., Vol. 25, n° 1, 1977, pp. 33-42.

LEMAITRE J., CHABOCHE J.-L., *Mécanique des Matériaux solides*, Dunod, 1988.

MARINI B., MUDRY F., PINEAU A.; "Ductile rupture of A508 steel under nonradial loading", Engineering Fracture Mechanics, vol. 22, 1985, pp. 375-386.

PILVIN P., Identification des paramètres de modèles de comportement, *Proc. Mécamat*, Besançon, 1988, pp 155-164.

RICE J. R., TRACEY D. M.; "On the ductile enlargement of voids in triaxial stress fields", Journal of the Mechanics and Physics of Solids, vol. 17, 1969, pp. 201-217.